JOM, Vol. 75, No. 10, 2023
https://doi.org/10.1007/s11837-023-06041-9
© 2023 The Author(s)

Finite Element Analysis of Additively Manufactured Continuous Carbon Fiber-Reinforced Composites

CHENSONG DONG [1,2]

1.—School of Civil and Mechanical Engineering, Curtin University, GPO Box U1987, Perth, WA 6845, Australia. 2.—e-mail: c.dong@curtin.edu.au

The objective of this study is to provide a numerical modeling approach for continuous carbon fiber (CCF)-reinforced fused filament fabricated composites. Although these materials have been extensively studied, an effective numerical modeling technique for their mechanical performance does not exist. To fill this technical gap, a numerical modeling approach based on finite element analysis is presented. The effective material properties of the Onyx matrix when voids are present are derived by the Kerner model. The material properties of CCF-reinforced composites are modeled by Hashin's model. Both the flexural and tensile properties are simulated. The modeling approach is validated against various experimental results.

INTRODUCTION

Additive manufacturing (AM), also known as 3D printing, can be used to make a wide range of parts with complex geometries and excellent design flexibility. Fused filament fabrication (FFF) or fused deposition modeling (FDM) is a widely used AM method for making composite materials. In this process, composite parts are made by applying the melted mixture material through an extrusion into layer-by-layer filaments.[1] The advantages include process flexibility, robustness and reliability, low material wastage, and low cost of printers and consumables. Several reviews on FFF have been published.[2–5] The Mark One and Mark Two printers developed by Markforged print continuous carbon fiber (CCF)-reinforced nylon with mechanical properties an order of magnitude higher than the unreinforced one.[6] The introduction of continuous fiber filaments can enhance the properties of 3D printed composites. For CCF-reinforced composites, the effect of fiber orientation was studied by Parmiggiani et al.[7] and Lupone et al.[8]

Finite element analysis (FEA)[9–12] has been employed to understand the behavior of composites. Galati et al.[9] presented a preliminary study based on 3D FEA for predicting the mechanical behavior of 3D-printed CCF-reinforced composites. Three fiber orientations were considered, aiming at the longitudinal, transverse, and shear moduli. The limitation is that only moduli in tension have been studied. In a study carried out by Polyzos et al.[11] on a numerical three-step multiscale model for 3D-printed FFF composites reinforced with continuous fibers, a good correlation of the analytical models for the micro- and mesoscale and to the experimental data for the macroscale was found. However, only elastic moduli were compared. Fu and Yao[12] presented a multiscale for 3D-printed continuous fiber-reinforced thermoplastic composites. Both the manufacturing process and mechanical properties were simulated and predicted. It is shown that these studies only modeled the tensile properties. Very limited studies have been conducted for the modeling of flexural properties. Krzikalla et al.[13] presented an experimental and numerical study on the flexural properties of AM composites. Only the linear portion of the flexural response was modeled.

It is shown from the literature that no effective numerical modeling technique is available for the mechanical performance of 3D-printed CCF-reinforced composites. In this study, an FEA-based modeling approach is presented. This model can predict both the flexural and tensile properties,

(Received December 20, 2022; accepted July 24, 2023; published online August 16, 2023)

including both the moduli and strengths. This modeling approach is validated against various experimental data, and it is shown that the model can accurately predict the moduli and strengths of 3D-printed CCF-reinforced composites.

METHODOLOGY

Material Properties

The composites in this study were printed by a Markforged Mark Two printer. This printer has two extrusion nozzles, one for Onyx and the other for continuous fiber-reinforced composites. Onyx is a nylon filament reinforced with chopped carbon fiber of $\sim 100\ \mu$m. The use of both chopped and continuous carbon fibers in 3D-printed (specifically FFF) composites offers several advantages, including enhanced mechanical properties, good printability, good design flexibility, and cost-effectiveness.

A bilinear plasticity-hardening model was used to describe the stress–strain relationship for Onyx. During the printing process, voids are formed between the filaments. To include the effect of voids, homogenization was carried out for the matrix and the voids. The effective modulus of the matrix with voids has been predicted using Kerner model:[14]

$$E_{\mathrm{me}} = \frac{9K_{\mathrm{me}}G_{\mathrm{me}}}{3K_{\mathrm{me}} + G_{\mathrm{me}}} \tag{1}$$

where G_{me} and K_{me} are the effective shear and bulk moduli of the matrix, respectively. The Kerner model has been chosen because its validity has been proven in a previous study.[15]

The effective shear modulus, G_{me}, is given by:

$$G_{\mathrm{me}} = G_m \frac{(7 - 5\nu_m)(1 - V_v)}{(7 - 5\nu_m) + (8 - 10\nu_m)V_v} \tag{2}$$

where G_m and ν_m are the void-free shear modulus and Poisson's ratio of the matrix, respectively, and V_v is the void content.

The effective bulk modulus, K_{me}, is given by:

$$K_{\mathrm{me}} = \frac{4G_mK_m(1 - V_v)}{4G_m + 3V_vK_m} \tag{3}$$

where K_m is the void-free bulk modulus.

The effective Poisson's ratio of the matrix when voids are present is:

$$\nu_{\mathrm{me}} = \frac{3K_{\mathrm{me}} - 2G_{\mathrm{me}}}{2(G_{\mathrm{me}} + 3K_{\mathrm{me}})} \tag{4}$$

Based on the void content in 3D-printed Onyx composites,[16] it is shown from the Kerner model that the effective modulus of Onyx is 1.963 GPa. The constants for the bilinear plasticity-hardening model are determined from the effective modulus of Onyx and previously published experimental results.[17] The model and experimental stress–strain curves for Onyx are shown in Fig. 1.

For the CCF-reinforced composite, its effective moduli are calculated from the properties of Onyx and carbon fiber[18] by Hashin's circular cylinder model (CCM).[19] Hashin's CCM has been widely used and is a recommended model for predicting the properties of composites.[20] The tensile modulus and strength of carbon fiber are taken to be 230 GPa and 4900 MPa, respectively. For a CCF composite ply, based on the constituent properties and its fiber volume fraction, the lamina properties, including the longitudinal modulus E_{11} and the shear moduli G_{12}, G_{13}, and G_{23}, are derived by Hashin's CCM.[19] The transverse moduli, E_{22} and E_{33}, are derived from the stress–strain relationship.[21]

The material properties of Onyx and the CCF-reinforced composite supplied by Markforged[22] are given in Table I. The fiber volume fraction of the CCF-reinforced composite was determined by back-calculation via the rule of mixtures from the tensile modulus to be 26%. This is in good agreement with a previous experimental study.[6]

The longitudinal tensile and compressive strength components of composites have been derived from various models.[23] The longitudinal tensile strength is given by:

$$S_{\mathrm{LT}} = E_{11}\varepsilon_{\mathrm{fu}} \tag{5}$$

where E_{11} is the longitudinal modulus and $\varepsilon_{\mathrm{fu}}$ is the failure strain of carbon fiber.

The longitudinal compressive strength is highly dependent on the failure mode. The experimental study by Tang et al.[16] on the longitudinal compression failure of 3D-printed CCF-reinforced

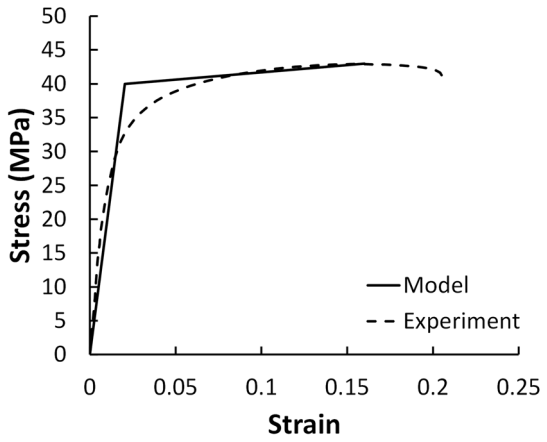


Fig. 1. Stress–strain curves for Onyx.

Table I. Material properties of Onyx and CCF-reinforced composite supplied by Markforged

	Onyx	CCF composite
Tensile modulus (GPa)	2.4	60
Tensile strength (MPa)	37	800
Compressive modulus (GPa)	–	54
Compressive strength (MPa)	–	320

composites shows that the composite specimen fails in the typical buckling mode. For the micro-buckling or kinking mode, the Lo-Chim model[24] was chosen to predict the longitudinal compressive strength. Its validity has been proven in our previous studies.[18,25] According to the Lo-Chim model, the longitudinal compressive strength is given by:

$$S_{LC} = \frac{G_{12}}{1.5 + 12\left(\frac{6}{\pi}\right)^2 \frac{G_{12}}{E_{11}}} \quad (6)$$

where G_{12} is the longitudinal–transverse shear modulus.

The tensile and compressive strengths calculated from Eqs. 5 and 6 are 1298 MPa and 496 MPa, respectively, which are significantly higher than those being supplied by Markforged. Strength reduction factors have been introduced to correct the predicted strengths. The strength reduction in longitudinal tension is mainly due to insufficient bonding between the carbon fiber and Onyx. The strength reduction in longitudinal compression is mainly due to the presence of voids, which can be estimated by the regression model presented in a previous study.[15] The strength reduction factors for the CCF composite are determined to be 0.62 for tension and 0.65 for compression.

For the transverse and shear strengths, because they are mostly matrix-dominant, the transverse tensile strength is estimated to be the strength of the matrix, the transverse compressive strength is estimated to be three times the strength of the matrix, and the shear strength is estimated to be 1.5 times the strength of the matrix. These estimates are based on some available experimental data.[26]

Stress-based failure criteria have been employed for failure prediction. When failure occurs in a ply, stiffness degradation factors[27] are used to reduce the stiffness. The stiffness degradation factor has been chosen to be 0.9.

Model Development

Ansys Workbench was employed to simulate 3D-printed CCF-reinforced composites under both flexural and tensile loadings. The composite specimen was modeled using Ansys ACP Pre (Ansys Composite Pre-processor). The composite was then exported as a shell to Ansys Mechanical to conduct a static structural analysis.

For the flexural properties, the composite specimen was supported by two rollers at a span of L and loaded at its mid-span. The span-to-thickness ratio was chosen to be 32. The hybrid composite was modeled as a shell structure and the supporting and loading rollers as cylindrical solids, as shown in Fig. 2. The shell was chosen for the efficiency of computation. Fixed support was applied to the supporting rollers and a pre-scribed displacement to the loading roller. Frictional contact was defined between the rollers and the composite specimen.

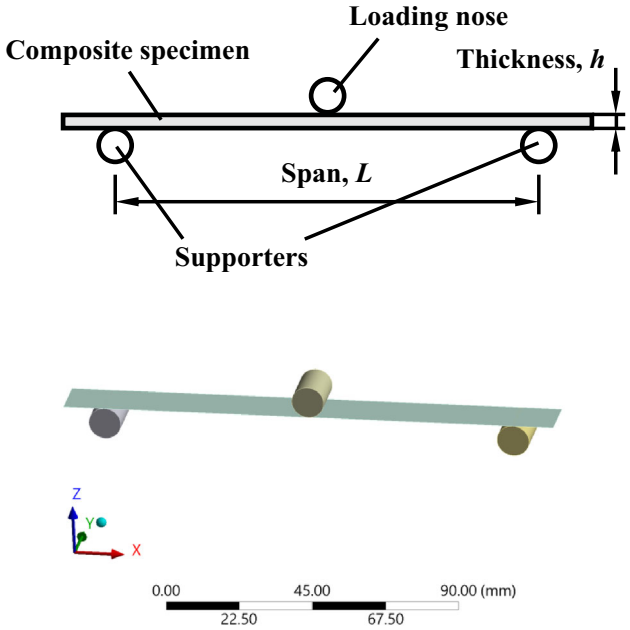


Fig. 2. A composite specimen in three-point bending.

Nonlinear analysis was conducted, and the force–displacement curve obtained upon completion of simulation. This developed modeling approach was validated against the experimental data.[25]

The failure load was determined from the load–displacement curve. Because the stress distribution is uniform in compression but non-uniform in bending, from Weibull statistical theory,[28] the flexural strength was about 30% higher than the compressive strength. Thus, the maximum bending load was also increased by 30%. According to procedure A of ASTM D7264/D7264M-15,[29] the flexural strength (S_F) is given by:

$$S_F = \frac{3P_{max}}{2bh^2} \quad (7)$$

and the flexural modulus (E_F) is given by:

$$E_F = \frac{\Delta\sigma_F}{\Delta\varepsilon_F} \quad (8)$$

where L, b, and h are the span, width, and depth of the specimen, respectively, D is the maximum deflection before failure, P_{max} is the maximum load encountered before failure, σ_F is the flexural stress, and ε_F is the flexural strain.

For the tensile properties, the composite specimen contained two tabs on each end, as shown in Fig. 3. Fixed support was applied to one tab and a prescribed displacement to the other tab. Linear analysis was conducted, and the force–displacement curve obtained upon completion of the simulation.

According to ASTM D3039/D3039M-17,[30] the tensile strength (S_T) is given by:

$$S_T = \frac{P_{max}}{bh} \quad (9)$$

And the tensile modulus (E_T) is given by:

$$E_T = \frac{\Delta\sigma_T}{\Delta\varepsilon_T} \tag{10}$$

where b and h are the width and thickness of the specimen, respectively, P_{max} is the maximum load encountered before failure, σ_T is the tensile stress, and ε_T is the tensile strain.

This FEA-based model was validated against the experimental results from a study on CCF-reinforced 3D-printed composites.[7] The flexural specimens contained 32 layers of pure Onyx or CCF/Onyx, and the tensile specimens contained 24 layers. The thickness of each layer was 0.125 mm. For all the specimens, the top and bottom four layers were pure Onyx, and the other layers were CCF/Onyx. The detailed layups are given in Table II.

Secondly, the model was validated against the experimental results from another study on CCF-reinforced 3D-printed composites.[8] The tensile properties of four layups: $[0]_S$, $[0/90]_S$, $[0/45/90/\pm 45]_S$, and $[0/\pm 60]_S$ were simulated.

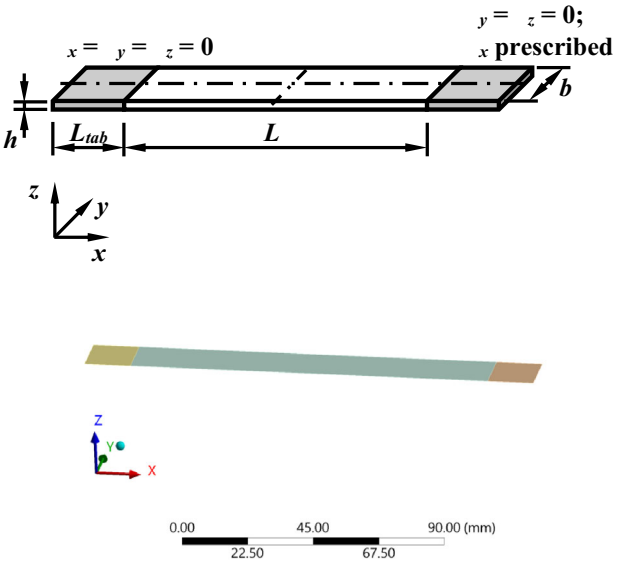


Fig. 3. A composite specimen in tension.

RESULTS

Flexural Properties

For each simulation for the flexural properties, the force, displacement, and maximum failure criterion were obtained from FEA. As an example, the deformation and maximum failure criteria of $[0/\pm 45]_6$ for flexural loading are given in the Electronic Supplementary Material (refer to online supplementary material). The deformation in the z direction is shown in Fig. S1 and the maximum failure criteria are shown in Fig. S2. A failure criterion greater than 1 means that failure has occurred. The stress–strain curves from FEA are shown in Fig. 4.

For the CCF-reinforced 3D-printed composites,[7] the flexural strengths and flexural moduli from the experiments and FEA are shown in Fig. 5, from which it can be seen that the FEA predictions are in good agreement with the experimental results. Except for $[90]_{24}$, the flexural strength from FEA is lower than that from the experiments, with the relative difference being in the range 7–20%. For the flexural modulus, the largest different is seen for $[90]_{24}$, for which the FEA prediction is 20% higher than the experimental result. For $[0]_{24}$, the FEA prediction is 7% higher than the experimental result, while for $[45]_{24}$, the FEA prediction is 14% lower than the experimental result. The relative differences for the other layups are lower than 4%.

Tensile Properties

Similar to the simulations for the flexural properties, for each simulation for the tensile properties, the force, displacement, and maximum failure criterion were obtained from FEA. As an example, the deformation and maximum failure criteria of $[0/\pm 45]_6$ for tensile loading are given in the Electronic Supplementary Material. The deformation in the x direction is shown in Fig. S3 and the maximum failure criteria are shown in Fig. S4. A failure criterion greater than 1 means failure has occurred. The stress–strain curves from FEA are shown in Fig. 6.

For the CCF-reinforced 3D-printed composites,[7] the tensile strengths and tensile moduli from the

Table II. Layups for flexural and tensile properties

Flexural properties			Tensile properties		
Layup	**Onyx layers**	**CCF layers**	**Layup**	**Onyx layers**	**CCF layers**
$[0]_{24}$	8	24	$[0]_{16}$	8	16
$[45]_{24}$	8	24	$[45]_{16}$	8	16
$[90]_{24}$	8	24	$[90]_{16}$	8	16
$[0/90]_{12}$	8	24	$[0/90]_8$	8	16
$[\pm 45]_{12}$	8	24	$[\pm 45]_8$	8	16
$[0/90/\pm 45]_6$	8	24	$[0/90/\pm 45]_4$	8	16
$[0/45/90/-45]_6$	8	24	$[0/45/90/-45]_4$	8	16

experiments and FEA are shown in Fig. 7, from which it can be that in general the FEA predictions for the tensile strength are in good agreement with the experimental results. For the tensile modulus, the FEA predictions are higher than the experimental results.

For the CCF-reinforced 3D-printed composites from another study,[8] the tensile properties from FEA simulation and experiments are shown in Fig. 8. For the tensile modulus, the FEA predictions are in good agreement with the experimental results, with the relative differences within 10%. For the tensile strength, good agreement is found for $[0]_S$ and $[0/45/90/\pm 45]_S$, with the relative differences less than 10%. For $[0/90]_S$, and $[0/\pm 60]_S$, the FEA prediction is about 30% higher than the experimental result.

Reinforcing Efficiency

With the aid of the developed modeling approach, the reinforcing efficiency of CCF-reinforced composite layers has been investigated. Both flexural and tensile properties were obtained from simulation by varying the number of CCF-reinforced composite layers. The flexural specimens consisted of 32 layers, including 4 roof Onyx layers and 4 floor Onyx layers. The CCF-reinforced composite layers were placed next to the roof and floor layers. The flexural strengths and moduli versus the number of CCF layers are shown in Fig. 9, from which it can be seen that the general trend is both the flexural strength and flexural modulus increasing with the number of CCF layers. The most significant increase in the flexural strength occurs when there are 8 CCF layers, and this is in agreement with a previous study.[31]

The tensile specimens consisted of 24 layers, including 4 roof Onyx layers and 4 floor Onyx layers. The CCF-reinforced composite layers were placed next to the roof and floor layers. The tensile strengths and moduli versus the number of CCF layers are shown in Fig. 10, from which it can be seen that both the tensile strength and tensile modulus linearly increase with the number of CCF layers.

CONCLUSION

This paper presents a comprehensive FEA-based numerical modeling approach for both the flexural and tensile properties of 3D-printed CCF-reinforced

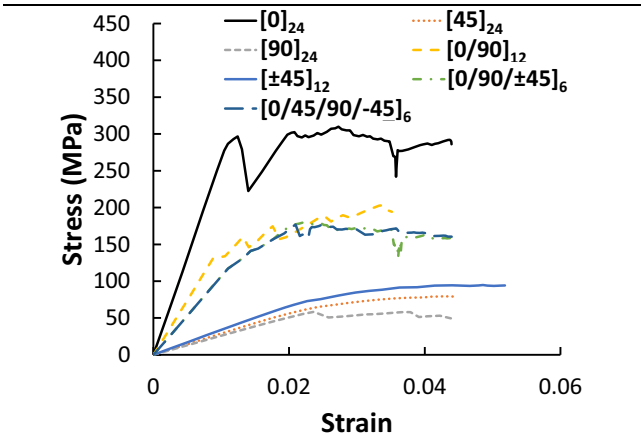


Fig. 4. Stress–strain curves for flexural loading.

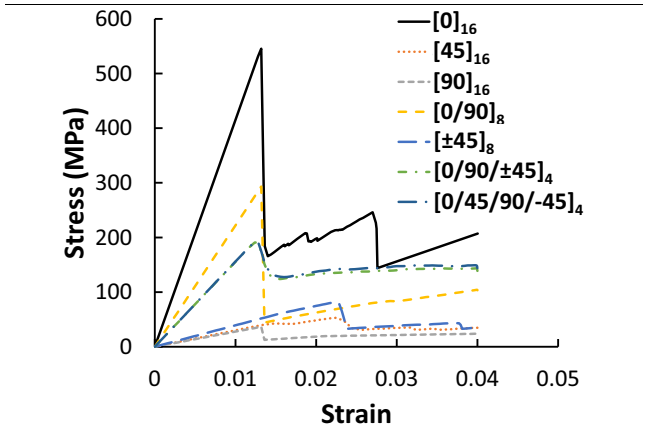


Fig. 6. Stress–strain curves for tensile loading.

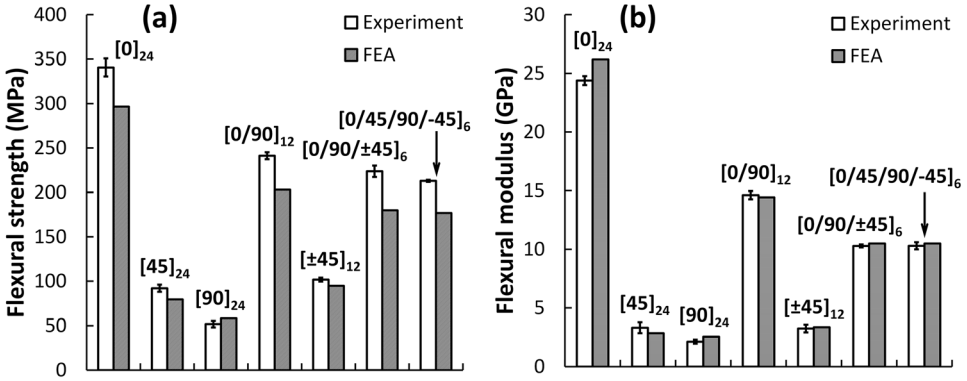


Fig. 5. (a) Flexural strengths and (b) flexural moduli from experiments and FEA for various layups (from Parmiggiani et al.[7]).

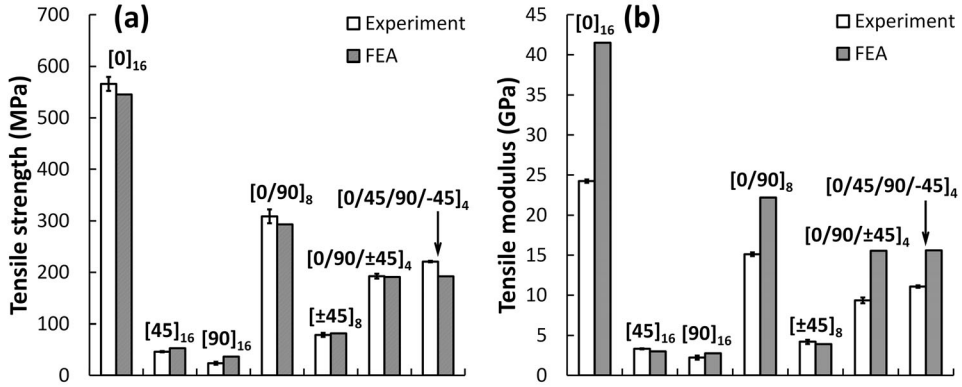


Fig. 7. (a) Tensile strengths and (b) tensile moduli from experimenta and FEA for various layups (from Parmiggiani et al.[7]).

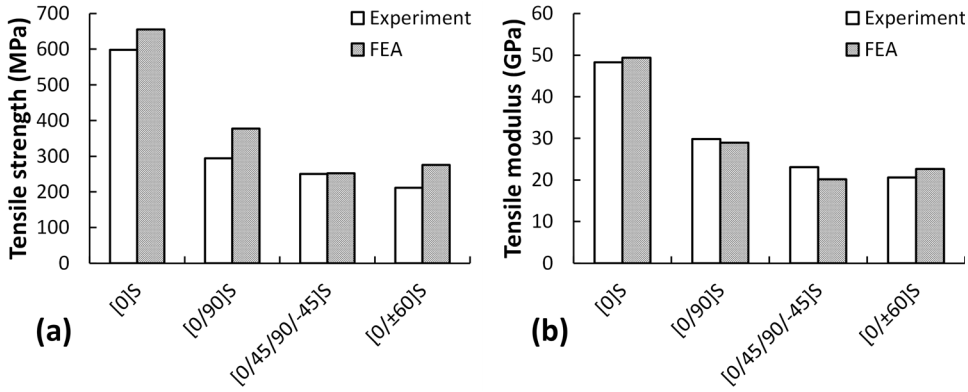


Fig. 8. (a) Tensile strengths and (b) tensile moduli from experiments and FEA for various layups (from Lupone et al.[8]).

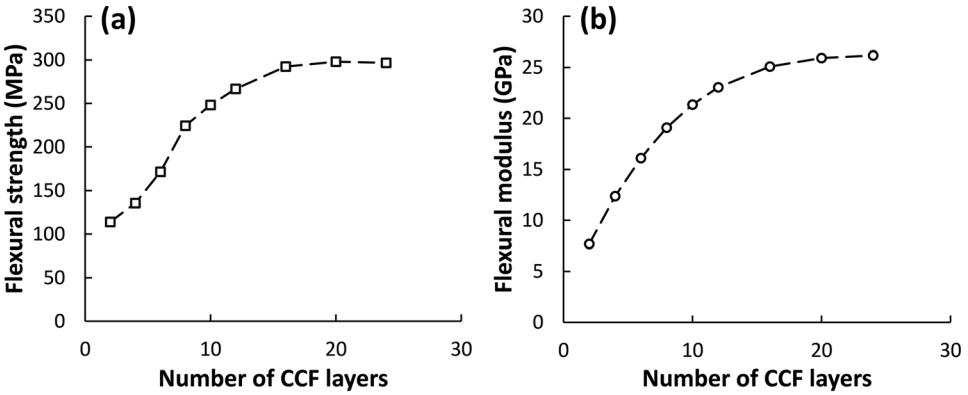


Fig. 9. (a) Flexural strength and (b) flexural modulus versus the number of CCF layers.

composites. This is the first time that such an approach has been developed. By comparing the FEA predictions with experimental results, it is shown that the relative differences are mostly within 20%, and thus the developed FEA modeling approach can predict the flexural and tensile behaviors of 3D-printed CCF composites with good accuracy. For a specimen consisting of 32 layers, the most significant improvement in the flexural strength occurs when there are 8 CCF-reinforced composite layers.

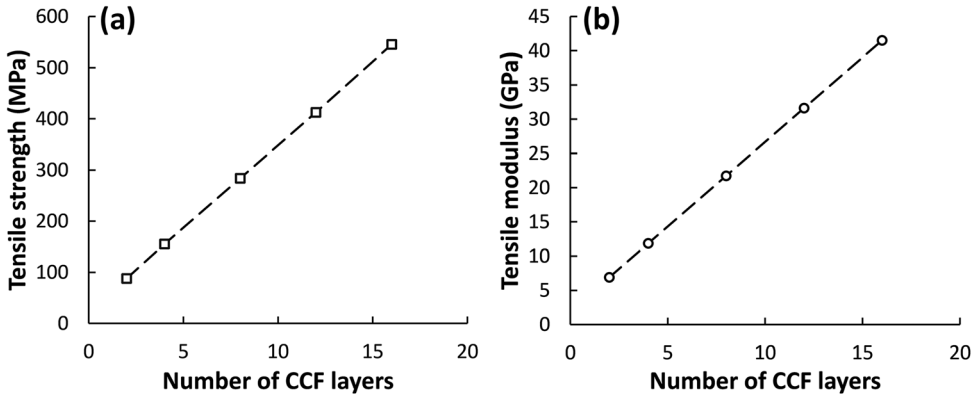


Fig. 10. (a) Tensile strength and (b) tensile modulus versus the number of CCF layers.

SUPPLEMENTARY INFORMATION

The online version contains supplementary material available at https://doi.org/10.1007/s11837-023-06041-9.

FUNDING

Open Access funding enabled and organized by CAUL and its Member Institutions. The authors did not receive support from any organization for the submitted work.

DATA AVAILABILITY

All data generated or analyzed during this study are included in this published article.

CONFLICT OF INTEREST

The authors declare that they have no conflict of interest.

OPEN ACCESS

This article is licensed under a Creative Commons Attribution 4.0 International License, which permits use, sharing, adaptation, distribution and reproduction in any medium or format, as long as you give appropriate credit to the original author(s) and the source, provide a link to the Creative Commons licence, and indicate if changes were made. The images or other third party material in this article are included in the article's Creative Commons licence, unless indicated otherwise in a credit line to the material. If material is not included in the article's Creative Commons licence and your intended use is not permitted by statutory regulation or exceeds the permitted use, you will need to obtain permission directly from the copyright holder. To view a copy of this licence, visit http://creativecommons.org/licenses/by/4.0/.

REFERENCES

1. Y. Wang, Y. Zhou, L. Lin, J. Corker, and M. Fan, Overview of 3D additive manufacturing (AM) and corresponding AM composites. *Compos. Part A Appl. Sci. Manuf.* 139, 106114 https://doi.org/10.1016/j.compositesa.2020.106114 (2020).
2. I. Ferreira, M. Machado, F. Alves, and A. Torres Marques, A review on fibre reinforced composite printing via FFF. *Rapid Prototyp. J.* https://doi.org/10.1108/RPJ-01-2019-0004 (2019).
3. S.M.F. Kabir, K. Mathur, and A.-F.M. Seyam, A critical review on 3D printed continuous fiber-reinforced composites: history, mechanism, materials and properties. *Compos. Struct.* 232, 111476 https://doi.org/10.1016/j.compstruct.2019.111476 (2020).
4. N. van de Werken, H. Tekinalp, P. Khanbolouki, S. Ozcan, A. Williams, and M. Tehrani, Additively manufactured carbon fiber-reinforced composites: state of the art and perspective. *Addit. Manuf.* 31, 100962 https://doi.org/10.1016/j.addma.2019.100962 (2020).
5. S. Yuan, S. Li, J. Zhu, and Y. Tang, Additive manufacturing of polymeric composites from material processing to structural design. *Compos. Part B Eng.* 219, 108903 https://doi.org/10.1016/j.compositesb.2021.108903 (2021).
6. L.G. Blok, M.L. Longana, H. Yu, and B.K. Woods, An investigation into 3D printing of fibre reinforced thermoplastic composites. *Addit. Manuf.* 22, 176 https://doi.org/10.1016/j.addma.2018.04.039 (2018).
7. A. Parmiggiani, M. Prato, and M. Pizzorni, Effect of the fiber orientation on the tensile and flexural behavior of continuous carbon fiber composites made via fused filament fabrication. *Int. J. Adv. Manuf. Technol.* 114, 2085 https://doi.org/10.1007/s00170-021-06997-5 (2021).
8. F. Lupone, E. Padovano, C. Venezia, and C. Badini, Experimental characterization and modeling of 3D printed continuous carbon fibers composites with different fiber orientation produced by FFF process. *Polymers* 14, 426 https://doi.org/10.3390/polym14030426 (2022).
9. M. Galati, M. Viccica, and P. Minetola, A finite element approach for the prediction of the mechanical behaviour of layered composites produced by continuous filament fabrication (CFF). *Polym. Test.* 98, 107181 https://doi.org/10.1016/j.polymertesting.2021.107181 (2021).
10. Z. Hou, X. Tian, J. Zhang, L. Zhe, Z. Zheng, D. Li, A.V. Malakhov, and A.N. Polilov, Design and 3D printing of continuous fiber reinforced heterogeneous composites. *Compos. Struct.* 237, 111945 https://doi.org/10.1016/j.compstruct.2020.111945 (2020).
11. E. Polyzos, D. van Hemelrijck, and L. Pyl, Numerical modelling of the elastic properties of 3D-printed specimens of

thermoplastic matrix reinforced with continuous fibres. *Compos. Part B Eng.* 211, 108671 https://doi.org/10.1016/j.compositesb.2021.108671 (2021).
12. Y. Fu and X. Yao, Multi-scale analysis for 3D printed continuous fiber reinforced thermoplastic composites. *Compos. Sci. Technol.* 216, 109065 https://doi.org/10.1016/j.compscitech.2021.109065 (2021).
13. D. Krzikalla, J. Měsíček, R. Halama, J. Hajnyš, M. Pagáč, T. Čegan, and J. Petrů, On flexural properties of additive manufactured composites: experimental, and numerical study. *Compos. Sci. Technol.* 218, 109182 https://doi.org/10.1016/j.compscitech.2021.109182 (2022).
14. E.H. Kerner, The elastic and thermo-elastic properties of composite media. *Proc. Phys. Soc. Lond. Sect. B* 69, 808 https://doi.org/10.1088/0370-1301/69/8/305 (1956).
15. C. Dong, Effects of process-induced voids on the properties of fibre reinforced composites. *J. Mater. Sci. Technol.* 32, 597 https://doi.org/10.1016/j.jmst.2016.04.011 (2016).
16. H. Tang, Q. Sun, Z. Li, X. Su, and W. Yan, Longitudinal compression failure of 3D printed continuous carbon fiber reinforced composites: an experimental and computational study. *Compos. Part A Appl. Sci. Manuf.* 146, 106416 https://doi.org/10.1016/j.compositesa.2021.106416 (2021).
17. C. Ma, J. Faust, and J.D. Roy-Mayhew, Drivers of mechanical performance variance in 3D-printed fused filament fabrication parts: an Onyx FR case study. *Polym. Compos.* 42, 4786 https://doi.org/10.1002/pc.26187 (2021).
18. C. Dong, H.A. Ranaweera-Jayawardena, and I.J. Davies, Flexural properties of hybrid composites reinforced by S-2 glass and T700S carbon fibres. *Compos. B Eng.* 43, 573 https://doi.org/10.1016/j.compositesb.2011.09.001 (2012).
19. T.-W. Chou, *Microstructural design of fiber composites* (Cambridge University Press, Cambridge, 1992).
20. J.P. Watt, G.F. Davies, and R.J. O'Connell, The elastic properties of composite materials. *Rev. Geophys.* 14, 541 https://doi.org/10.1029/RG014i004p00541 (1976).
21. Z. Hashin, Analysis of composite materials—a survey. *J. Appl. Mech.* 50, 481 https://doi.org/10.1115/1.3167081 (1983).
22. Markforged. Composites material datasheet, https://static.markforged.com/downloads/composites-data-sheet.pdf. Accessed 26 June 2022.
23. C. Dong, Uncertainties in flexural strength of carbon/glass fibre reinforced hybrid epoxy composites. *Compos. B Eng.* 98, 176 https://doi.org/10.1016/j.compositesb.2016.05.035 (2016).
24. K.H. Lo and E.S.-M. Chim, Compressive strength of unidirectional composites. *J. Reinf. Plast. Compos.* 11, 838 https://doi.org/10.1177/073168449201100801 (1992).
25. C. Dong, Flexural properties of symmetric carbon and glass fibre reinforced hybrid composite laminates. *Compos. Part C Open Access* 3, 100047 https://doi.org/10.1016/j.jcomc.2020.100047 (2020).
26. P.K. Mallick, *Fiber-reinforced composites: materials, manufacturing, and design*, 2nd edn. (Marcel Dekker, New York, 1993).
27. M.R. Garnich and V.M.K. Akula, Review of degradation models for progressive failure analysis of fiber reinforced polymer composites. *Appl. Mech. Rev.* https://doi.org/10.1115/1.3013822 (2008).
28. R.E. Bullock, Strength ratios of composite materials in flexure and in tension. *J. Compos. Mater.* 8, 200 https://doi.org/10.1177/002199837400800209 (1974).
29. Standard Test Method for Flexural Properties of Polymer Matrix Composite Materials.
30. Standard Test Method for Tensile Properties of Polymer Matrix Composite Materials.
31. J.M. Chacón, M.A. Caminero, P.J. Núñez, E. García-Plaza, I. García-Moreno, and J.M. Reverte, Additive manufacturing of continuous fibre reinforced thermoplastic composites using fused deposition modelling: effect of process parameters on mechanical properties. *Compos. Sci. Technol.* 181, 107688 https://doi.org/10.1016/j.compscitech.2019.107688 (2019).

Publisher's Note Springer Nature remains neutral with regard to jurisdictional claims in published maps and institutional affiliations.